Intermediate mass Higgs boson at the proposed CERN LEP⊗LHC *ep* collider. I. Standard model

Ghadir Abu Leil
Department of Physics, University of Durham, South Road, Durham DH1 3LE, United Kingdom

Stefano Moretti*
Department of Physics, University of Durham, South Road, Durham DH1 3LE, United Kingdom and Dipartimento di Fisica Teorica, Università di Torino, and INFN, Sezione di Torino, V. Pietro Giuria 1, 10125 Torino, Italy

(Received 16 March 1995; revised manuscript received 24 July 1995)

The production of the SM Higgs boson ϕ with intermediate mass at the proposed CERN LEP ⊗ LHC *ep* collider in $\gamma q(\bar{q}) \to W^{\pm}\phi q'(\bar{q}')$, $\gamma q(\bar{q}) \to Z^0\phi q(\bar{q})$, and $g\gamma \to q\bar{q}\phi$ events is studied. This is done for all possible (massive) flavors of the quarks $q(q')$ and using photons generated via Compton back scattering of laser light. We study signatures in which the Higgs boson decays to $b\bar{b}$ pairs and the electroweak vector bosons $W^{\pm}$ and Z^0 decay either hadronically or leptonically. All possible backgrounds to these signals are also computed. Flavor identification on b jets is assumed. Explicit formulas for helicity amplitudes of the above processes are given.

PACS number(s): 14.80.Bn, 13.60.Fz, 14.65.Fy

INTRODUCTION

The Higgs sector is one of the most investigated parts of the standard model (SM) [1,2], yet it continues to be very elusive. So far the Higgs particle has evaded all searches. Nevertheless, a lower limit on the mass of the SM Higgs boson ϕ of ≈ 60 GeV was extracted from the lack of $e^+e^- \to Z^0 \to Z^{0*}\phi$ events at the CERN e^+e^- collider LEP I [3]. An upper bound of ≈ 1 TeV is expected. This was derived by requiring the validity of perturbation theory [4] and the unitarity of the model [5]. Therefore, if the SM Higgs boson ϕ exists, we could expect it to be discovered by the next generation of CERN high energy colliders: LEP II ($\sqrt{s_{ee}} = 160$–200 GeV) [6] and the Large Hadron Collider (LHC) ($\sqrt{s_{pp}} = 10, 14$ TeV) [7].

LEP II will be able to cover the mass range $M_\phi < 80$–100 GeV. A Higgs boson with a larger mass should be searched for at the LHC. At LEP II ϕ can be detected[1] through a large variety of decay channels, the most favored being $Z^0\phi \to (\mu^+\mu^-)(b\bar{b})$. A Higgs boson with mass $M_\phi \gtrsim 130$ GeV is clearly detectable at the LHC using the four-lepton mode[2] $\phi \to Z^0Z^0 \to l\bar{l}l\bar{l}$. Because of the QCD backgrounds typical of hadron colliders, it is still controversial whether it is possible to detect an intermediate mass Higgs[3] boson in the mass range $90 \lesssim M_\phi \lesssim 130$ GeV (where ϕ mainly decays to $b\bar{b}$ pairs). In this mass range ϕ can be searched for through the rare $\gamma\gamma$ decay mode and this relies on the fact that both a high luminosity and a very high diphoton mass resolution must be achieved at the LHC [15]. It is also unclear whether it is possible to cleanly detect the intermediate SM Higgs boson in the $\phi \to b\bar{b}$ channel using the b-tagging capabilities of vertex detectors [16,17]. The main difficulties being the expected low signal rates after reconstruction, the necessity to have an accurate control on all the possible background sources and to achieve a very high b-tagging performance [18].

In the distant future, cleaner environments for studying the Higgs boson parameters will be the e^+e^- linear accelerators ($\sqrt{s_{ee}} = 350$–2000 GeV) [19–23].

At the Next Linear Collider (NLC), with $\sqrt{s_{ee}} = 300$–500 GeV [22], the Higgs boson can be searched for through a large number of channels over the whole intermediate mass range [24]. The dominant production mechanism is the Bjorken reaction for $\sqrt{s_{ee}}$ below 500 GeV while the $W^{\pm}W^{\pm}$ and Z^0Z^0 fusion processes [25] will dominate at larger energies. At $\sqrt{s_{ee}} \gtrsim 500$ GeV [21] a heavy Higgs boson can be detected in the four-jet modes $\phi \to W^{\pm}W^{\mp}, Z^0Z^0 \to jjjj$ [26,27] in addition to the $4l$ mode. At higher energies, $\sqrt{s_{ee}} = 1$–2 TeV [23], the same search strategies still hold with the fusion mechanisms becoming the dominant ones.

The conversion of the linear e^+e^- NLC's into $\gamma\gamma$ and/or $e\gamma$ colliders, by photons generated via Compton back scattering of laser light, will provide new possibilities for detecting and studying the Higgs boson [28]. In $\gamma\gamma$ collisions two of the important channels will be the production of a heavy Higgs boson (up to ≈ 350 GeV) by a triangular loop of heavy fermions or $W^{\pm}$, with the detection via the decay mode $\phi \to Z^0Z^0 \to q\bar{q}l^+l^-$ at $\sqrt{s_{ee}} = 500$ GeV [29], and the process $\gamma\gamma \to t\bar{t}\phi$, which appears more useful than the corresponding e^+e^- one in

*Present address: Cavendish Laboratory, University of Cambridge, Madingley Road, Cambridge, CB3 0HE, U.K.

[1]And produced via the Bjorken bremsstrahlung process $e^+e^- \to Z^{0*} \to Z^0\phi$ [8].

[2]With ϕ produced via gg [9] or $W^{\pm}W^{\mp}$ and Z^0Z^0 fusion [10].

[3]Via the associated production with a $W^{\pm}$ boson (decaying leptonically to $l\nu$) [11,12] or a $t\bar{t}$ pair (with one t decaying semileptonically to $bl\nu$) [13,14].

measuring the top Yukawa coupling $t\phi$, at $\sqrt{s_{ee}} = 1$–2 TeV [30]. The $e\gamma$ option at linear colliders can be exploited for studying Higgs boson production via the process $e\gamma \to \nu_e W\phi$, at $\sqrt{s_{ee}} = 1$–2 TeV and over the mass range 60 GeV $\lesssim M_\phi \lesssim$ 150 GeV [31,32], using the signature $W^-\phi \to (jj)(b\bar{b})$ [33]. The cross section for the above process at such $\sqrt{s_{ee}}$'s is comparable to the fusion processes $e^+e^- \to \bar{\nu}_e\nu_e W^{\pm *}W^{\mp *} \to \bar{\nu}_e\nu_e\phi$ and larger than the bremsstrahlung reaction $e^+e^- \to Z^{0*} \to Z^0\phi$. Finally, it has been shown in Ref. [34] that the process $e\gamma \to e\gamma\gamma \to e\phi$ is the most important mechanism for ϕ production at $\sqrt{s_{ee}} = 500$ GeV, for $M_\phi \gtrsim 140$ GeV.

Let us now consider the production of the SM Higgs boson at *ep* machines. This seems to be beyond the capabilities of the DESY *ep* collider HERA [35], which has been primarily designed for providing accurate data on the proton structure functions in the small-x region, more than for Higgs boson searches [36]. In the future, another *ep* collider is contemplated, the CERN LEP⊗LHC accelerator: it will combine an electron or positron beam from LEP II and a proton beam from the LHC [7,37]. A detailed study on the detectability of an intermediate mass SM Higgs boson at such a machine has been presented in Ref. [38]. This is based on the $W^\pm W^\mp$ and Z^0Z^0 fusion processes [36,39,40], with ϕ decaying to $b\bar{b}$. It has been shown that it should be possible to detect ϕ provided that a high luminosity and/or an excellent b-flavor identification can be achieved. Only recently has the possibility of resorting to back-scattered laser photons at the *ep* CERN collider been suggested [41], searching for, e.g., $\gamma q \to q'W^\pm\phi$ events, with $\phi \to b\bar{b}$ and $W^\pm \to l\nu$ or jj, which should give detectable Higgs boson signals if good $M_{b\bar{b}}$ invariant mass resolution can be achieved and efficient b tagging can be performed.

The purpose of this paper is to study the following reactions at the LEP⊗LHC *ep* collider:

$$q\gamma \to q'W^\pm\phi\,, \tag{1}$$

$$q\gamma \to qZ^0\phi\,, \tag{2}$$

$$g\gamma \to q\bar{q}\phi\,, \tag{3}$$

in the intermediate mass range of ϕ, for all possible (anti)flavors of the (anti)quarks $q(q')$, using laser backscattered photons. We discuss their relevance to the detection of the SM Higgs boson and the study of its parameters, with the Higgs boson decaying to $b\bar{b}$ pairs and assuming flavor identification on its decay products.

Although process (1) has already been studied in [41], and the part of the analysis devoted to it here largely overlaps that study, we decided nevertheless to include it for completeness and since, in principle, we can slightly improve the results previously obtained. In fact, since we consider heavy quarks we include additional Higgs boson bremsstrahlung off quarks in the amplitudes, even though these are suppressed with respect to contributions coming from diagrams involving ϕW^+W^- vertices. We also computed all the necessary rates for all the relevant backgrounds exactly, whereas these latter contributions were only estimated in [41]. Reaction (3) has been analyzed in [42] for the minimal supersymmetric SM (MSSM) neutral Higgs bosons, b quarks and using bremsstrahlung photons but to our knowledge, neither the larger energy option available at LEP⊗LHC nor the possibility of using laser backscattered photons has been exploited.

There are at least two important motivations for analyzing processes (1)–(3) at the LEP⊗LHC collider. First, if the SM Higgs boson turns out to have an intermediate mass greater than the maximum value that can be reached by LEP II and if the LHC detectors are not able to achieve the necessary performances for the predicted Higgs boson measurements [18], the *ep* CERN collider will be the first alternative option available for studying such a Higgs boson, as it will certainly be operating before any NLC. Second, although both the cross sections and the luminosity at LEP⊗LHC are expected to be small if compared with the LHC ones, the CERN *ep* option will constitute the first TeV energy environment partially free from the enormous QCD background typical of purely hadronic colliders. Moreover, processes (1)–(3) have the advantage, compared to the $W^\pm W^\mp$ and Z^0Z^0 fusion mechanisms, that the additional heavy particles $W^\pm$ and Z^0 (and also t, in principle) can be used for tagging purposes by searching for their decays, thus increasing the signal to background ratio.

The plan of the paper is as follows. In Sec. II we give details of the calculation and the numerical values adopted for the various parameters. Section III is devoted to the discussion of the results, while the conclusions are in Sec. IV. The helicity amplitudes for processes (1)–(3) are presented in the Appendix.

CALCULATION

Figure 1 shows all the Feynman diagrams at tree level contribution to the reactions (1) and (2) in the unitary gauge, where (q, q', V) represent the possible combinations (d, u, W^-), (u, d, W^+), and (q, q, Z^0), respectively [in the case of process (2) only the first eight diagrams of Fig. 1 contribute]. Figure 2 shows the Feynman diagrams at tree level for process (3). All quarks have been considered massive, so diagrams with a direct coupling of ϕ to the fermion lines have been taken into account.

The amplitudes squared have been computed by means of the spinor techniques of Refs. [43,44] and, as a check, also by the method of Ref. [45]. The matrix elements for the processes $\bar{d}\gamma \to \bar{u}W^+\phi/\bar{u}\gamma \to \bar{d}W^-\phi$ and $\bar{q}\gamma \to \bar{q}Z^0\phi$ can easily be obtained by trivial operations of charge conjugation. All of the above amplitudes have been tested for gauge invariance. We were also able to "roughly"[4] reproduce, with appropriate couplings, hadron distributions, and luminosity function of the photons, the results of Ref. [41] and of Ref. [42]. Moreover, since a simple adaptation of the implemented formulas (by changing photon couplings from quarks into leptons and setting

[4]See footnote 9 below.

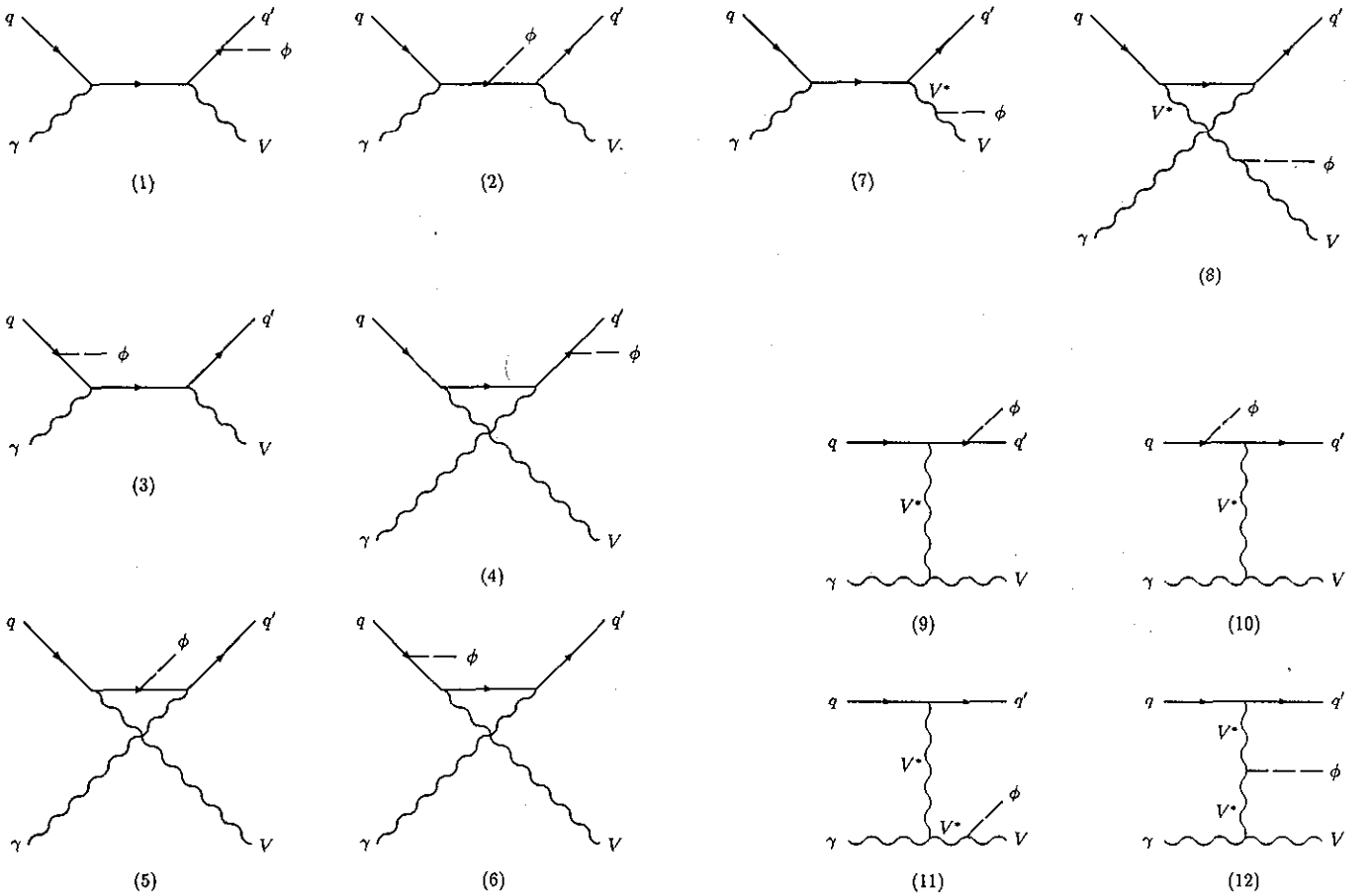

FIG. 1. Feynman diagrams contributing in lowest order to $q\gamma \to q'V\phi$, where $q(q')$ represents a quark, $V(V^*)$ an external (internal) vector boson and ϕ the SM Higgs boson, in the unitary gauge. In the case $V = Z^0$ and $q' = q$ only the first eight diagrams of Fig. 1 contribute.

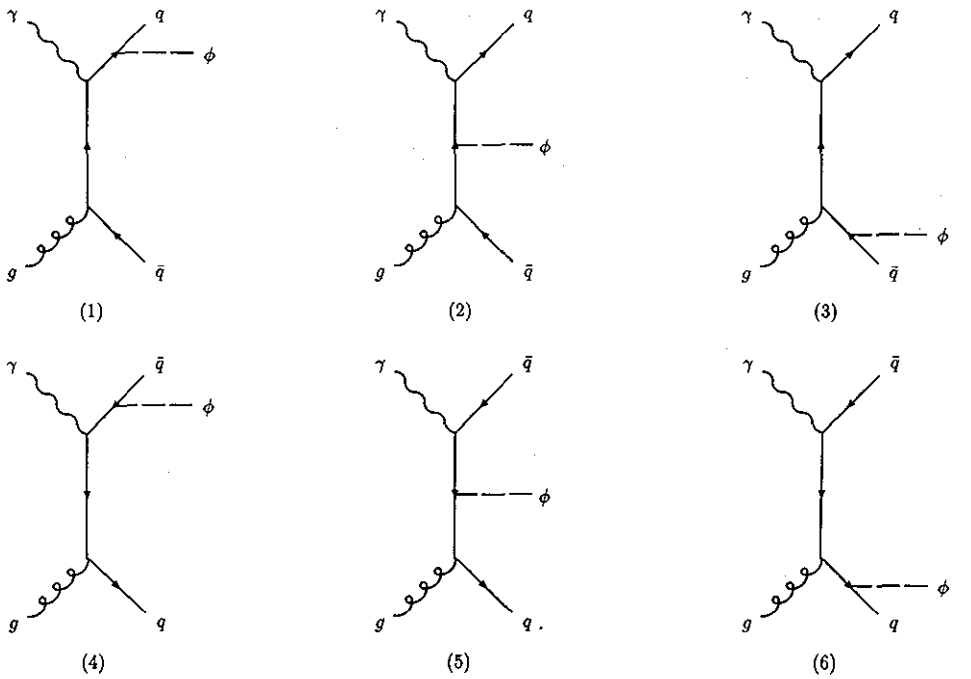

FIG. 2. Feynman diagrams contributing in the lowest order to $g\gamma \to q\bar{q}\phi$, where q represents a quark and ϕ the SM Higgs boson, in the unitary gauge.

the quark masses equal to zero) allowed us to reproduce the computation of Ref. [33], we have checked our helicity amplitudes in this way also.

As proton structure functions we adopted the Harriman-Martin-Roberts-Stirling (HMRS) set B [46] (this was done in order to make comparison with already published work easier), setting the energy scale equal to the center-of-mass (c.m.) energy at the parton level (i.e., $\mu = \sqrt{\hat{s}_{\rm parton}}$). The strong coupling constant α_s, which appears in the gluon initiated processes, has been evaluated at two loops, for $\Lambda_{\rm QCD} = 190$ MeV, with a number $N_f = 5$ of active flavors and a scale μ equal to that used for the proton structure functions. We are confident that changing the energy scale and/or distribution function choice should not affect our results by more than a factor[5] of 2.

For the energy spectrum of the back-scattered (unpolarized) photon we have used [49]

$$F_{\gamma/e}(x) = \frac{1}{D(\xi)}\left[1 - x + \frac{1}{1-x} - \frac{4x}{\xi(1-x)} + \frac{4x^2}{\xi^2(1-x)^2}\right], \tag{4}$$

where $D(\xi)$ is that renormalization factor

$$D(\xi) = \left(1 - \frac{4}{\xi} - \frac{8}{\xi^2}\right)\ln(1+\xi) + \frac{1}{2} + \frac{8}{\xi} - \frac{1}{2(1+\xi)^2}, \tag{5}$$

and $\xi = 4E_0\omega_0/m_e^2$, ω_0 is the incoming laser photon energy, and E_0 the (unpolarized) electron or positron energy. In Eq. (4) $x = \omega/E_0$ is the fraction of the energy of the incident electron or positron carried by the back-scattered photon, with a maximum value

$$x_{\rm max} = \frac{\xi}{1+\xi}. \tag{6}$$

In order to maximize ω while avoiding e^+e^- pair creation, one takes ω_0 such that $\xi = 2(1+\sqrt{2})$ and one gets the typical values $\xi \simeq 4.8, x_{\rm max} \simeq 0.83, D(\xi) \simeq 1.8$.

In the case of $q(g)\gamma$ scattering from ep collisions, the total cross section σ is obtained by folding the subprocess cross section $\hat{\sigma}$ with the photon $F_{\gamma/e}$ and hadron $F_{q(g)/p}$ luminosities:

$$\sigma(s_{ep}) = \int_{x^\gamma_{\rm min}}^{x^\gamma_{\rm max}} dx^\gamma \int_{x^{q(g)}_{\rm min}}^{1-x^\gamma} dx^{q(g)} F_{\gamma/e}(x^\gamma) F_{q(\bar{g})/p}(x^{q(g)}) \hat{\sigma}(\hat{s}_{q(g)\gamma} = x^\gamma x^{q(g)} s_{ep}), \tag{7}$$

where $\hat{s}_{q(g)\gamma}$ is the c.m. energy at parton [i.e., $q(g)\gamma$] level, while

$$x^\gamma_{\rm min} x^{q(g)}_{\rm min} = \frac{(M_{\rm final})^2}{s_{ep}}, \tag{8}$$

where $M_{\rm final}$ is the sum of the final state particle masses.

The multidimensional integrations have been performed numerically using the Monte Carlo routine VEGAS [48].

To our knowledge, a detailed study, as for the cases of $e\gamma$ and $\gamma\gamma$ collisions [49], on the efficiency of the laser back-scattering method in converting $e \to \gamma$ at ep colliders does not exist. In this paper we assume for the effective γp luminosity the same as the ep one, therefore the conversion efficiency of electrons into backscattered γ's is one. For the discussions of the results we have adopted an overall total integrated luminosity $\mathcal{L} = 3$ fb^{-1} per year, the value of Ref. [41].

For the numerical part of our work, we have taken $\alpha_{\rm em} = 1/128$ and $\sin^2\theta_W \equiv s_W^2 = 0.23$, while for the gauge boson masses and widths: $M_{Z^0} = 91.175$ GeV, $\Gamma_{Z^0} = 2.5$ GeV, $M_{W^\pm} = M_{Z^0}\cos\theta_W \equiv M_{Z^0}c_W$, and $\Gamma_{W^\pm} = 2.2$ GeV. For the fermions we have $m_e = 0.511 \times 10^{-3}$ GeV, $m_\mu = 0.105$ GeV, $m_\tau = 1.78$ GeV, $m_u = 8.0 \times 10^{-3}$ GeV, $m_d = 15.0 \times 10^{-3}$ GeV, $m_s = 0.3$ GeV, $m_c = 1.7$ GeV, $m_b = 5.0$ GeV, and $m_t = 175$ GeV [50], with all widths equal to zero apart from $\Gamma_t \approx 1.58$ GeV, adopting its tree-level expression. All neutrinos have been considered massless: i.e., $m_{\nu_e} = m_{\nu_\mu} = m_{\nu_\tau} = 0$. The branching ratios (BR's) of the Higgs boson were extracted from Ref. [51].

We have analyzed the processes (1)–(3) over the mass range 60 GeV $\lesssim M_\phi \lesssim$ 140 GeV and for ep c.m. energy ranging from 0.5 to 3.0 TeV, with special attention devoted to the case $\sqrt{s_{ep}} = 1.36$ TeV, corresponding to the collision of an electron or positron beam from LEP II and a proton beam from LHC [41].

RESULTS

In Figs. 3–5 we present the dependence of processes (1)–(3) on the collider c.m. energy, for a selection of Higgs masses: $M_\phi = 60, 80, 100, 120$, and 140 GeV. Summations over all possible combinations of (anti)flavors have been performed (the top contributions in the final states are included[6]), as well as the integration over the initial $g/q(\bar{q})$ and γ structure functions. A general feature in Figs. 3 and 5 is the rapid increase of all the plots with $\sqrt{s_{ep}}$, especially for $\sqrt{s_{ep}} \gtrsim 1$ TeV. This is because for $\sqrt{s_{ep}}$ much larger than the final particle masses,

[5] We verified this in few cases by comparing the actual results to the ones obtained from the more recent set of structure functions MRS(A) [47].

[6] As a first approximation only combinations of two flavors within the same quark doublet have been computed for process (1), setting all Cabibbo-Kobayashi-Maskawa terms equal to one.

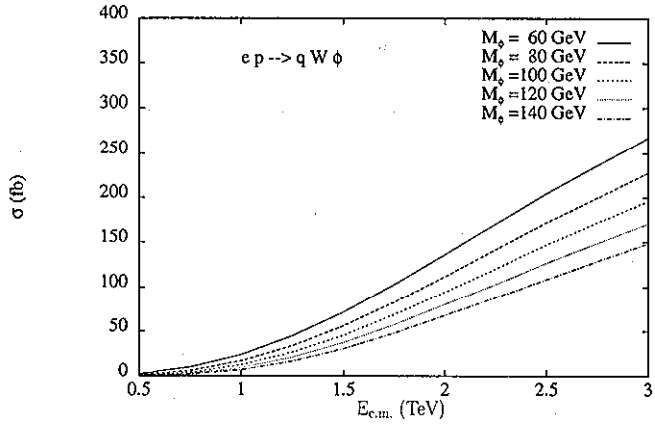

FIG. 3. Cross sections of process (1) as a function of $\sqrt{s_{ep}}$, for a selection of Higgs boson masses. The HMRS(B) structure functions are used.

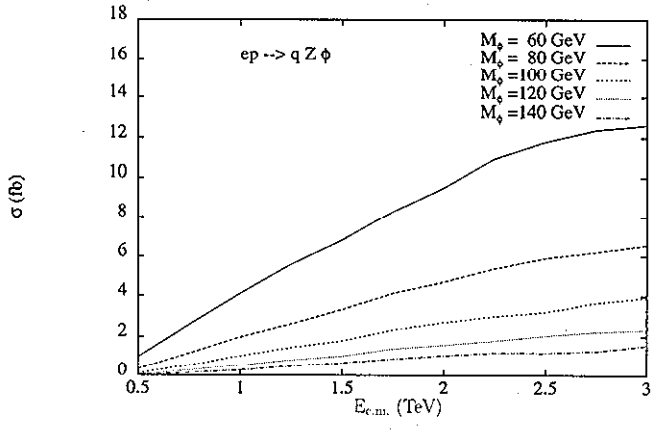

FIG. 4. Cross sections of process (2) as a function of $\sqrt{s_{ep}}$, for a selection of Higgs boson masses. The HMRS(B) structure functions are used.

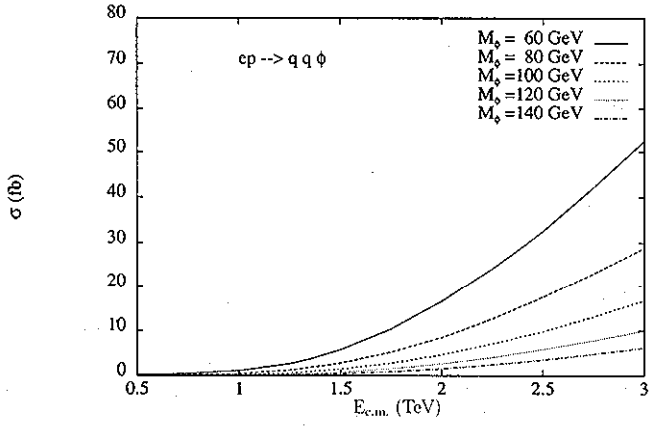

FIG. 5. Cross sections of process (3) as a function of $\sqrt{s_{ep}}$, for a selection of Higgs boson masses. The HMRS(B) structure functions are used.

TABLE I. Production cross sections for processes (1)–(3), at $\sqrt{s_{ep}} = 1.36$ TeV, with $M_\phi = 60$, 80, 100, 120, and 140 GeV. The HMRS(B) structure functions are used. The errors are the statistical errors on the numerical calculation.

	σ (fb)		
M_ϕ (GeV)	$q'W^\pm\phi$	$qZ^0\phi$	$q\bar{q}\phi$
60	55.61 ± 0.34	6.13 ± 0.10	3.806 ± 0.058
80	42.84 ± 0.25	3.056 ± 0.052	1.765 ± 0.029
100	34.53 ± 0.14	1.581 ± 0.028	0.872 ± 0.013
120	27.56 ± 0.11	0.798 ± 0.024	0.4513 ± 0.0068
140	22.048 ± 0.080	0.547 ± 0.018	0.2419 ± 0.0039
	$\sqrt{s} = 1.36$ TeV HMRS(B)		

phase space effects are quantitatively unimportant. The same effect is less evident in Fig. 4, since process (2) is affected by the s-channel structure of the corresponding Feynman diagrams, whereas [part of] these are in t channel for process [(1)](3). We also notice that the cross section for the process $ep \to W^\pm\phi X$ is much larger than that of $ep \to Z^0\phi X$. This is due to two reasons: first, the coupling ϕW^+W^- is larger than $\phi Z^0 Z^0$ and second, in process (1) there are additional diagrams (i.e, 9–12 in Fig. 1), some of which (i.e., 11 and 12) are not suppressed by Yukawa couplings.

In Table I we give the cross sections at the LEP⊗LHC c.m. energy $\sqrt{s_{ep}} = 1.36$ TeV. To show the importance of the relative contributions of the various flavors entering in the subprocesses (1)–(3), we give their separate rates in Table II at $M_\phi = 60$ GeV. For reaction (1) at a fixed $\sqrt{s_{ep}}$, increasing the Higgs boson mass reduces the top quark contributions, this is due to the limited phase space available, while the light flavors contributions (i.e., $q = u, d, s, c$, and b) do not change significantly. For example, the top contribution to process (1) diminishes from 1.4% to 0.12% when M_ϕ increases from 60 to 140 GeV, whereas the contributions from *up* (*down*) [*strange*] {*charm*}-initiated processes vary from $\approx$ 53(35)[8]{3}% to $\approx$ 64(29)[5]{2}%. For process (2) there is no substantial phase space effect of this kind, since we cannot have top contributions here. Thus the numbers do not differ as much: they are $\approx$ 74(16)[4]{5}⟨0.6⟩% to $\approx$ 80(14)[3]{3}⟨0.33⟩%, with the numbers in the "brackets" ⟨ ⟩ corresponding to b contributions. For reaction (3), things change dramatically because, on the one hand, top lines are not connected to the initial state as in (1) and the phase space suppression due to the large top mass is important only if $\sqrt{s_{ep}} \lesssim 1$ TeV, and on the other hand, the Higgs boson always couples to the very massive top quark through the ($\sim m_t$) Yukawa coupling, in all Feynman diagrams at tree level. Because of this $\sim m_q$ coupling the very light flavors $q = u$, d, and s give here completely negligible contributions, while c and b fractions are suppressed by a factor of $\approx (m_t/m_c)^2 \approx 10^4$ and $\approx (m_t/m_b)^2 \approx 1225$, with respect to the top ones. Therefore, for process (3), the top contribution is by far the dominant one for $\sqrt{s_{ep}} \gtrsim 1$ TeV and all ϕ masses.[7]

[7]Whereas for $\sqrt{s_{ep}} \lesssim 1$ TeV the c contribution is the largest one: in this case the effect of the $q\gamma$ electromagnetic coupling, which favors c quarks, is dominant on the Yukawa $q\phi$ electroweak one, which favors b quarks.

The corresponding numbers at the LEP⊗LHC energy, varying M_ϕ in the range 60–140 GeV, are $\approx$ 0.0016–0.0013 % for u, $\approx$ 0.0013–0.0011 % for d, $\approx$ 0.29–0.28 % for s, $\approx$ 17–20 % for c, $\approx$ 14–21 % for b, and $\approx$ 69–58 % for t quarks.

Next, we checked if neglecting diagrams 1–6 [and 9–10] of process (2)[(1)] inside the matrix elements, as done in Ref. [41], where all quark masses were set equal to zero, could be a source of error.[8] In doing this we needed to apply some cuts to avoid collinear and soft singularities (in the couplings of the incoming photon to the outgoing quark $q_{\rm out}$) that would otherwise make our amplitudes divergent. To do this, we require, e.g., $|\cos\theta_{\gamma q_{\rm out}}| < 0.95$ and $|p_{q_{\rm out}}| > 3$ GeV: restrictions which are reasonably compatible with eventual requirements from the detectors.[9] Setting again $\sqrt{s_{ep}} = 1.36$ TeV and $M_\phi = 60$ GeV, we have found percentage differences only of the order of 1 in 1000 in the case of light flavor final states, and of $\approx 2\%$ for the contribution $b\gamma \to tW^-\phi$+c.c., in process (1). For reaction (2), differences are appreciable only in the case of c and b quarks, these being $\approx 3\%$ and $\approx 13\%$, respectively. These mass effects are approximately the same over the whole intermediate M_ϕ range. However, because of the relative flavor contributions of Tables II(a) and II(b), when one sums over all of these the effects are largely washed out. We also notice that the errors due to neglecting the quark masses are larger for process (2) than for (1), since in the latter there are also contributions (dominant with respect to the Higgs bremsstrahlung) coming from $\gamma \to W^+W^-$ splitting whereas at tree level there is no corresponding $\gamma \to Z^0Z^0$ coupling. Obviously, taking into account the masses in process (3) is crucial, since there the Higgs is always produced through the Yukawa couplings $q\phi$.

We know that in the mass range 60 GeV $\lesssim M_\phi \lesssim$ 140 GeV the dominant Higgs decay mode is $\phi \to b\bar{b}$. The corresponding BR in the above interval varies from ≈ 0.85 at $M_\phi = 60$ GeV to ≈ 0.38 at $M_\phi = 140$ GeV, where the off-shell $W^{\pm *}W^{\mp}$ decay channel begins to be competitive [51]. So, in order to maximize the number of signal events we look for the $\phi \to b\bar{b}$ signature. We further require flavor identification of b jets, exploiting the possibilities offered by b-tagging techniques, to reduce the large QCD backgrounds.

In processes (1)–(3) we have additional decaying particles[10]: a $W^\pm$ in $q\gamma \to q'W^\pm\phi$, a Z^0 in $q\gamma \to qZ^0\phi$, and two t's in the $g\gamma \to t\bar{t}\phi$ contribution. So we expect the following possible final signatures[11]:

TABLE II. Production cross sections for processes (1)–(3) in (a)–(c), respectively, at $\sqrt{s_{ep}} = 1.36$ TeV, with $M_\phi = 60$ GeV, for all different flavor combinations entering in the partonic subprocesses. The HMRS(B) structure functions are used. The errors are the statistical errors on the numerical calculation.

(a)

Flavors	σ (fb)
$u\gamma \to dW^+\phi + \bar{u}\gamma \to \bar{d}W^-\phi$	29.58 ± 0.15
$d\gamma \to uW^-\phi + \bar{d}\gamma \to \bar{u}W^+\phi$	19.37 ± 0.30
$s\gamma \to cW^-\phi + \bar{s}\gamma \to \bar{c}W^+\phi$	4.228 ± 0.021
$c\gamma \to sW^+\phi + \bar{c}\gamma \to \bar{s}W^-\phi$	1.620 ± 0.012
$b\gamma \to tW^-\phi + \bar{b}\gamma \to \bar{t}W^+\phi$	0.7995 ± 0.0033
$\sqrt{s} = 1.36$ TeV HMRS (B)	$M_\phi = 60$ GeV

$\sqrt{s} = 1.36$ TeV HMRS(B) $M_\phi = 60$ GeV

(b)

Flavors	σ (fb)
$u\gamma \to uZ^0\phi + \bar{u}\gamma \to \bar{u}Z^0\phi$	4.535 ± 0.097
$d\gamma \to dZ^0\phi + \bar{d}\gamma \to \bar{d}Z^0\phi$	0.982 ± 0.025
$s\gamma \to sZ^0\phi + \bar{s}\gamma \to \bar{s}Z^0\phi$	0.2707 ± 0.0015
$c\gamma \to cZ^0\phi + \bar{c}\gamma \to \bar{c}Z^0\phi$	0.3018 ± 0.0012
$b\gamma \to bZ^0\phi + \bar{b}\gamma \to \bar{b}Z^0\phi$	0.03839 ± 0.00017

$\sqrt{s} = 1.36$ TeV HMRS(B) $M_\phi = 60$ GeV

(c)

Flavors	σ (fb)
$g\gamma \to u\bar{u}\phi$	$(60.4 \pm 2.2) \times 10^{-6}$
$g\gamma \to d\bar{d}\phi$	$(51.09 \pm 0.83) \times 10^{-6}$
$g\gamma \to s\bar{s}\phi$	$(11.113 \pm 0.071) \times 10^{-3}$
$g\gamma \to c\bar{c}\phi$	0.6572 ± 0.0025
$g\gamma \to b\bar{b}\phi$	0.5188 ± 0.0019
$g\gamma \to t\bar{t}\phi$	2.6192 ± 0.0049

$\sqrt{s} = 1.36$ TeV HMRS(B) $M_\phi = 60$ GeV

$$ep \to W^\pm\phi X \to (l\nu_l)(b\bar{b})X\ ,$$
$$ep \to Z^0\phi X \to (l\bar{l})(b\bar{b})X\ , \qquad (9)$$

or

$$ep \to W^\pm\phi X \to (jj)(b\bar{b})X\ ,$$
$$ep \to Z^0\phi X \to (jj)(b\bar{b})X\ , \qquad (10)$$

(where X represents the untagged particles in the final states) depending on whether the electroweak massive vector bosons decay leptonically or hadronically, respectively.[12] As for process (3) we expect the signature

$$ep \to q\bar{q}\phi X \to jj(b\bar{b})X \qquad (11)$$

for light quark contributions, and

[8] We expect differences coming from phase space effects to be negligible for the light flavors u, d, s, c, and b, since $m_q \ll \sqrt{s_{ep}}$ for all of them.

[9] Since similar cuts were not listed in Ref. [41], we were unable to reproduce exactly the numbers there computed.

[10] In principle, we also have t quarks in process (1) which could decay to bW pairs, but in practice, contributions involving top quarks are here generally quite small if compared to those of the other flavors and substantially negligible when we sum up all different combinations.

[11] We know that in all processes (1)–(3) we can have additional b's from t/Z^0 decays or $b\gamma/g\gamma$ fusion, but we assume that complications coming from the fact of taking in those events a wrong combination $b\bar{b}$ can be largely avoided if we restrict to keep $b\bar{b}$-invariant masses in the window $|M_{b\bar{b}} - M_\phi| < 5$ GeV (see later on).

[12] We do not exploit here possible missing energy decays $Z^0 \to \nu\bar{\nu}$ in process (2).

$$ep \to t\bar{t}\phi X \to b\bar{b}W^{\pm}(b\bar{b})X \qquad (12)$$

for top quarks [with $B(t \to bW) \approx 1$].

Therefore out of the $\approx$ 56–22[6–0.6] initial femtobarns of reaction (1)[(2)] at $\sqrt{s_{ep}} = 1.36$ TeV and for $M_\phi = 60$–140 GeV, assuming $\mathcal{L} = 3$ fb^{-1}, we expect $\approx$ 99–18[11–< 1] events for hadronic decays, and $\approx$ 42–8[2–< 1] for leptonic modes, whereas for reaction (3), starting from $\approx$ 3.8–0.24 fb, we end up with $\approx 10- < 1$ events (7 of these come from $t\bar{t}\phi$ production with $M_\phi = 60$ GeV) per year.

The irreducible backgrounds to the above signatures are $ep \to W^{\pm}Z^0X \to W^{\pm}(b\bar{b})X$ and $ep \to \bar{t}bX \to b\bar{b}W^{\pm}X$ for process (1), $ep \to Z^0Z^0X \to Z^0(b\bar{b})X$ for (2), and $ep \to q\bar{q}Z^0X \to q\bar{q}(b\bar{b})X$ for (3). These are always present, independently of the $W^{\pm}/Z^0$ decay modes in processes (1)–(2). In addition, multijet photoproduction, $W^{\pm}$+jets, Z^0+jets and $t\bar{t}X \to b\bar{b}W^{\pm}X$ production and decay events must be also considered.

A few remarks concerning the $t\bar{b}X$ background are needed here. We have mentioned earlier that we take the $e \to \gamma$ conversion efficiency ϵ (into back-scattered photons) equal to 1, which implies that all the incoming electrons are converted into photons and hence removed from the interaction site. This motivates us to consider γp initiated processes only, and not ep ones. Single-top production proceeds in γp collisions through the partonic subprocesses $q\gamma \to q'W^{\pm *}\gamma \to q't\bar{b} + q'\bar{t}b \to q'b\bar{b}W^{\pm}$ (i.e., via $\gamma W^{\pm}$ fusion) and $g\gamma \to tbW^{\pm} \to b\bar{b}W^{+}W^{-}$ (i.e., via $\gamma \to W^{+}W^{-}$ splitting and $g\gamma$ fusion), whereas in ep collisions it happens via $e^{-}g \to \nu_e W^{\pm *}g \to t\bar{b}\nu_e$. While this latter process has a very large cross section (approximately 1200 fb at $\sqrt{s_{ep}} = 1.36$ TeV), the sum of the first two gives rates generally at the level of one order of magnitude larger than the ones of the signal $qW^{\pm}\phi \to qW^{\pm}(b\bar{b})$, for $m_t = 175$ GeV (see below). Therefore, we would like to stress that it is extremely important that an efficiency ϵ greater than $\approx 90\%$ should be achievable, otherwise a non-negligible fraction $(1-\epsilon)$ of the single-top background proceedings via $W^{\pm}g$ fusion would enter in the experimental sample, inducing a strong suppression of the signal versus background ratio. In fact, the production rate of the $qW^{\pm}\phi$ signal via bremsstrahlung photons is more than ten times smaller than the one via backscattered γ's [41].

While b-tagging identification should drastically reduce the backgrounds where b quarks are not present in the final states, this requirement is not generally enough if they are. In this case, one has to look for invariant masses of the $b\bar{b}$ pair in a window around M_ϕ, since the most part of the signals lie within this region. In the case of top-resonant backgrounds (i.e., $\bar{t}bX$ and $t\bar{t}X$) we can also exploit the cut, e.g., $|M_{bW \to bjj} - m_t| > 15$ GeV, which should be very effective in reducing hadronic $W^{\pm}$ decays since top peaks are quite narrow (in fact, $\Gamma_t \approx 1.58$ GeV for $m_t = 175$ GeV). Finally, if the Higgs mass turns out to be close to the Z^0 mass, the precise absolute normalizations of the processes involving $M_{b\bar{b}}$ resonances are needed.

Assuming good b-tagging performances such that it is possible to drastically eliminate the non-b multijet photoproduction, $W^{\pm}$ + jets and Z^0 + jets background events [41], and that the $M_{b\bar{b}}$ cut is sufficient to suppress the above processes in the case of $\gamma^*/g^* \to b\bar{b}$ splitting, we end up having to deal only with the backgrounds $ep \to W^{\pm}Z^0X \to W^{\pm}(b\bar{b})X$, $ep \to \bar{t}bX \to b\bar{b}W^{\pm}X$, $ep \to Z^0Z^0X \to Z^0(b\bar{b})X$, $ep \to t\bar{t}X \to b\bar{b}W^{\pm}X$, and $ep \to q\bar{q}Z^0X \to q\bar{q}(b\bar{b})X$. Moreover, we should not forget that an additional drastic rejection factor on the multijet background comes from requiring that $M_{jj}/M_{l\bar{\nu}_l,l\bar{l}}$ has to reproduce $M_{W^{\pm}}$ or M_{Z^0} for processes (1)–(2), and that $M_{bW \to bjj} \approx m_t$ for (3) when $q = t$ (since this flavor is by far the largest partonic contribution at the LEP⊗LHC energy).

TABLE III. Production cross sections for the background processes discussed in the text. The HMRS(B) structure functions are used. The errors are the statistical errors on the numerical calculation.

Background	σ (fb)
$ep \to W^{\pm}Z^0X$	224.3 ± 1.9
$ep \to \bar{t}bX \to b\bar{b}W^{\pm}X$	535.3 ± 5.1
$ep \to t\bar{t}X \to b\bar{b}W^{\pm}X$	1114.7 ± 1.4
$ep \to Z^0Z^0X$	12.15 ± 0.50
$ep \to q\bar{q}Z^0X$	3714 ± 91
$\sqrt{s} = 1.36$ TeV HMRS(B)	

In order to study the background rates, we have implemented their matrix elements in FORTRAN codes generated by MADGRAPH [52] and HELAS [53].[13] The total cross sections of these processes are displayed in Table III, at $\sqrt{s_{ep}} = 1.36$ TeV, for the same γ and $g/q(\bar{q})$ structure functions and parameters employed for the signal processes. We notice that backgrounds are in general much larger than the corresponding signals, both for the top-resonant cases (continuum backgrounds) and for the $Z^0 \to b\bar{b}$ ones (discrete backgrounds). While in the former case this happens because of the top-resonant peaks, in the latter we have that the qZ^0 coupling does not depend on the q mass (contrary to the Higgs one), so light quarks give large contributions here. This is especially evident in the case of the reaction $ep \to q\bar{q}Z^0$. The rates for $ep \to Z^0Z^0X$ are of the same order of magnitude as the signal $ep \to Z^0\phi X$: in this case the contributions from Z^0 bremsstrahlung off quarks in the background (we do not have triple vector boson vertices in this case) are comparable to those of the signal in which ϕ is emitted from a Z^0 line.

However, in principle these very large rates should not be a problem since processes $ep \to W^{\pm}Z^0X$, $ep \to Z^0Z^0X$, and $ep \to q\bar{q}Z^0X$ are really important only when $M_\phi \approx M_{Z^0}$, whereas $ep \to \bar{t}bX \to b\bar{b}W^{\pm}X$ and $ep \to t\bar{t}X \to b\bar{b}W^{\pm}X$ are highly reduced when applying a cut in the $b\bar{b}$-invariant mass (i.e., $M_{b\bar{b}} \approx M_\phi$) and eventually, for $W^{\pm}$ hadronic decays, also the cut $M_{bW} \approx m_t$

[13] Since process $ep \to t\bar{t}X \to b\bar{b}W^{\pm}X$ was already studied in Ref. [54], we also checked that the helicities amplitudes we obtained reproduce the results of that paper (for bremsstrahlung photons).

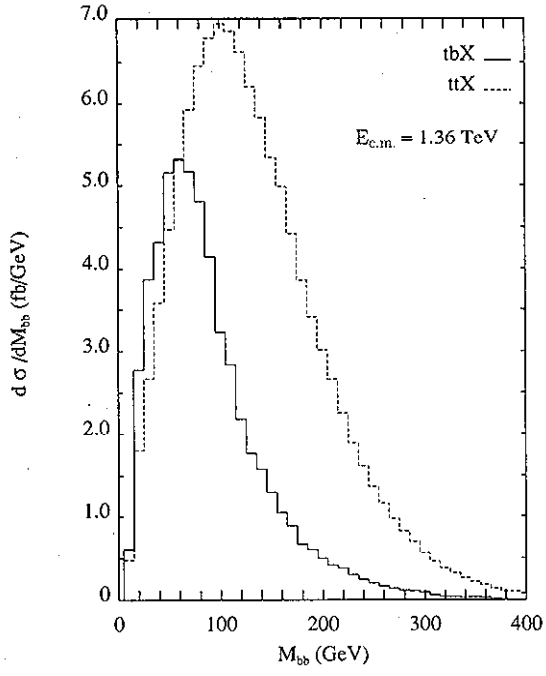

FIG. 6. Differential distributions in the invariant mass of the $b\bar{b}$-pair $M_{b\bar{b}}$ for the $\bar{t}bX \to b\bar{b}W^{\pm}X$ and $t\bar{t}X \to b\bar{b}W^{\pm}X$ backgrounds, at $\sqrt{s_{ep}} = 1.36$ TeV. The HMRS(B) structure functions are used.

can be used. In Fig. 6 we give the differential distributions in the invariant mass $M_{b\bar{b}}$ for those backgrounds in which the $b\bar{b}$ pair does not come from a Z^0 resonance: i.e., $\bar{t}bX \to b\bar{b}W^{\pm}X$ and $t\bar{t}X \to b\bar{b}W^{\pm}X$ ($W^{\pm}$ BR's are not included). For backgrounds containing a $Z^0 \to b\bar{b}$ resonance, we naively assume that all the $M_{b\bar{b}}$ spectrum is contained in the region $|M_{b\bar{b}} - M_{Z^0}| \leq 2\Gamma_{Z^0} = 5$ GeV.

Since we are concentrating on $b\bar{b}$-invariant masses in the M_ϕ region, we require that $M_{b\bar{b}}$ of all events is in the window $|M_{b\bar{b}} - M_\phi| < 5$ GeV, assuming that 10 GeV will be the mass resolution of the detectors. The fractions of the total cross sections from $\bar{t}bX$ and $t\bar{t}X$ production which pass this cut are given by the area under the $M_{b\bar{b}}$ distributions of Fig. 6 between $M_\phi - 5$ and $M_\phi + 5$ GeV, while we assume that those of the Z^0-resonant $b\bar{b}$ events are given by the formula [33]

$$\delta\sigma(Z^0) = \sigma(Z^0)\frac{\max(0, 10\text{ GeV} - |M_\phi - M_{Z^0}|)}{10\text{ GeV}} . \quad (13)$$

In using the above equation we tacitly assumed that the $\phi \to b\bar{b}$ peaks are also all contained in a region of 10 GeV around the ϕ pole.[14] The number of signal (S) and background (B) events and their statistical significance ($S/\sqrt{B}$) are given in Table IV, for the three processes (1)–(3) and the sum of their backgrounds separately, for the usual selection of ϕ masses, after the $M_{b\bar{b}}$ cut. BR's

[14]In fact, the Higgs boson width at $M_\phi = 140$ GeV is $\Gamma_\phi \approx 0.01$ GeV.

TABLE IV. Number of signal (S) and background events (B) and their statistical significance ($S/\sqrt{B}$), for the processes (1)–(3), at $\sqrt{s_{ep}} = 1.36$ TeV, in the window $|M_{b\bar{b}} - M_\phi| < 5$ GeV, for the usual selection of Higgs boson masses. Numbers correspond to hadronic (leptonic) decays of the $W^{\pm}/Z^0$'s. The HMRS(B) structure functions are used. The symbol "–" indicates the case in which the backgrounds do not constitute a problem in disentangling the signals.

Process	S	B	$S/\sqrt{B}$	M_ϕ (GeV)
$q'W^{\pm}\phi$	99(42)	418(179)	4.84(3.14)	
$qZ^0\phi$	11(2)	0(0)	–(–)	60
$q\bar{q}\phi$	10	0	–	
$q'W^{\pm}\phi$	75(32)	452(194)	3.53(2.30)	
$qZ^0\phi$	5(1)	0(0)	–(–)	80
$q\bar{q}\phi$	4	0	–	
$q'W^{\pm}\phi$	59(25)	412(177)	2.91(1.88)	
$qZ^0\phi$	3(0)	0(0)	–(0)	100
$q\bar{q}\phi$	2	196	0.14	
$q'W^{\pm}\phi$	41(17)	357(153)	2.17(1.37)	
$qZ^0\phi$	1(0)	0(0)	–(0)	120
$q\bar{q}\phi$	1	0	–	
$q'W^{\pm}\phi$	18(8)	300(128)	1.10(0.71)	
$qZ^0\phi$	0(0)	0(0)	0(0)	140
$q\bar{q}\phi$	0	0	0	

of hadronic and leptonic $W^{\pm}/Z^0$ decays, giving the signatures in Eqs. (9)–(12), are included both for processes (1)–(2) and for the backgrounds. We do not make any assumption about the $W^{\pm}$ decays when $q = t$ in process (3) and on the second $W^{\pm}$ in tbX and $t\bar{t}X$, treating them completely inclusively (i.e., such that $W^{\pm}$'s can decay either hadronically or leptonically).

As criteria for the observability of a signal, we require a rate $S \geq 6$ events with a significance $S/\sqrt{B} > 4$ for the detection of an isolated Higgs boson peak, while for the case of Higgs boson peaks overlapping with Z^0 peaks we require $S \geq 10$ with $S/\sqrt{B} > 6$ [33]. Table IV shows the rates for the signal (S) processes $q'W^{\pm}\phi, qZ^0\phi$ and $q\bar{q}\phi$ and their backgrounds (B) separately, together with the corresponding significances, whereas Table V summarizes the results when one tries to make an "inclusive" analysis, summing the rates for signals and backgrounds. Apart from the case $M_\phi \lesssim 80$ GeV for hadronic decays, the starting values of $S/\sqrt{B}$ in both situations are generally small. This happens because the largest signal (i.e., $W^{\pm}\phi X$) has a huge background, whereas the other two signals (i.e., $Z^0\phi X$ and $q\bar{q}\phi X$), even though virtually free from backgrounds, give very few events.

TABLE V. Total number of signal ($S_{\rm tot}$) and background events ($B_{\rm tot}$) and their statistical significance ($S_{\rm tot}/\sqrt{B_{\rm tot}}$), after summing the numbers in Table IV in "inclusive" rates.

$S_{\rm tot}$	$B_{\rm tot}$	$S_{\rm tot}\sqrt{B_{\rm tot}}$	M_ϕ (GeV)
120(44)	418(179)	5.87(3.32)	60
84(33)	452(194)	3.95(2.37)	80
64(26)	608(373)	2.60(1.35)	100
43(18)	357(153)	2.28(1.46)	120
19(8)	300(128)	1.10(0.71)	140

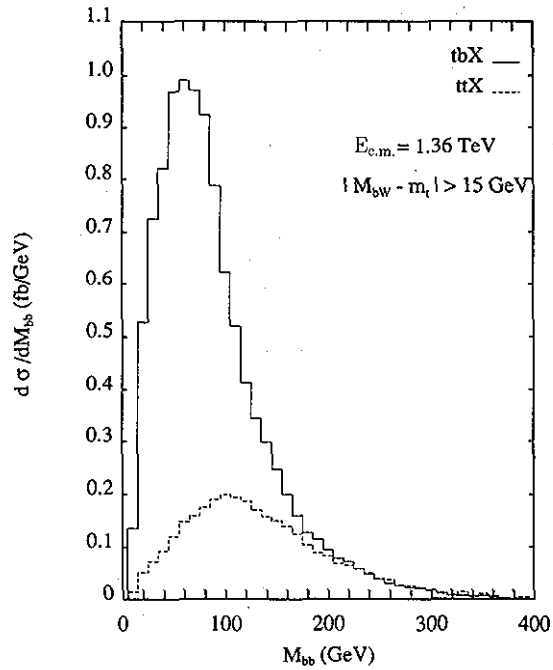

FIG. 7. Differential distributions in the invariant mass of the $b\bar{b}$-pair $M_{b\bar{b}}$ for the $\bar{t}bX \to b\bar{b}W^{\pm}X$ and $t\bar{t}X \to b\bar{b}W^{\pm}$ backgrounds, at $\sqrt{s_{ep}} = 1.36$ TeV, after the cut $|M_{bW\to bjj} - m_t| > 15$ GeV. The HMRS(B) structure functions are used.

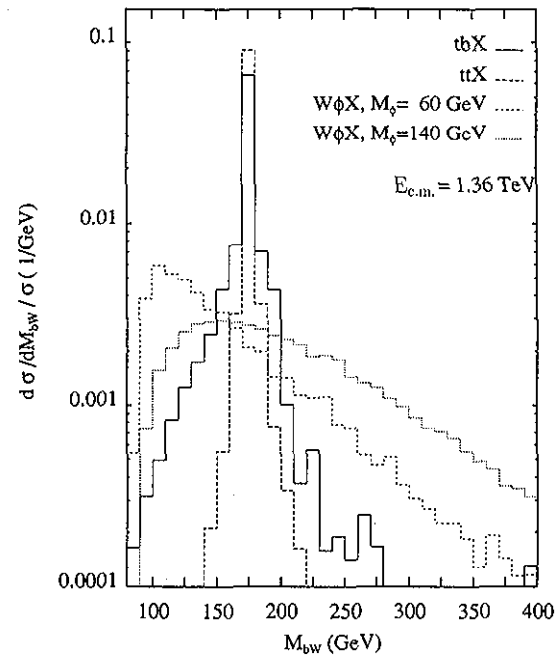

FIG. 8. Differential distributions in the invariant mass of the bW-system M_{bW} for the $\bar{t}bX \to b\bar{b}W^{\pm}X$ and $t\bar{t}X \to b\bar{b}W^{\pm}X$ backgrounds, and the signal $W^{\pm}\phi X \to W^{\pm}(b\bar{b})X$ with $M_\phi = 60$, 140 GeV, at $\sqrt{s_{ep}} = 1.36$ TeV. The HMRS(B) structure functions are used.

Therefore, it is clear already at this point that in the case of overlapping peaks it does not appear to be any possibility to disentangle the signals (see Tables I and III), even after a few years of running. However, when $|M_\phi - M_{Z^0}| \gtrsim 5$ GeV, region where only the continuum backgrounds are effective, one can exploit (in the case of hadronic $W^{\pm}$ decays) the restriction $|M_{bW\to bjj} - m_t| > 15$ GeV (for both the combinations bW^+ and $\bar{b}W^+$, assuming to tag the positive gauge boson). For this, in Fig. 7 we plot the differential distributions in $M_{b\bar{b}}$ of the $\bar{t}bX$ and $t\bar{t}X$ backgrounds, after applying the above M_{bW} cut. It is clear then how this cut turns out to be extremely useful in rejecting the continuum backgrounds, since their rates are now reduced of $\approx 81\%$ (for tbX) and of $\approx 97\%$ (for $t\bar{t}X$). If we insert these reduction factors in Tables IV and V (in which we have now to divide all B's by a factor of ≈ 13, and multiply all $S/\sqrt{B}$'s by $\approx \sqrt{13}$) the significances become larger than 4 over almost all the intermediate Higgs boson mass range ($M_\phi \lesssim 120$ GeV). At the same time, the reduction factor for $W^{\pm}\phi X$ is just a few percent, since the corresponding distribution in M_{bW} is nearly flat (see Fig. 8): e.g., approximately 7% for $M_\phi = 60$ GeV and 8% for $M_\phi = 140$ GeV.

A few comments concerning the mass resolution, $|M_\phi - M_{b\bar{b}}| < 5$ GeV, that we have used throughout this paper are worth mentioning at this point. In Ref. [38], a larger value was adopted. Here, the fact that we performed the analysis at the parton level would enable us to use for consistency a value of ≈ 7 GeV [18] (which corresponds to a resolution between 11 and 12.3 GeV at the jet level). In addition, it has to be remembered that the real performances of a possible ep CERN collider are not predictable at the moment, and it is not inconceivable that by the time the LEP⊗LHC machine comes into operation further progresses in resolving the mass spectra can be achieved. Therefore, for the time being, we deliberately chose a smaller and more optimistic value. However, if eventually it turns out that such a performance will not be feasible, the rates for a worse mass resolution (say 10 GeV) can be readily deduced from the ones given here. In fact, for the signals, due to the small Higgs width in the intermediate mass range, they remain practically unchanged. For the case of the discrete backgrounds we expect smaller significances only in the region around the Z^0 peak, where it is already impossible to disentangle Higgs signals for a mass resolution of 5 GeV. Finally, for the continuum backgrounds, the numbers would be roughly a factor 2 bigger (see Figs. 6 and 7). Therefore, an additional (overall) reduction factor of $\approx \sqrt{2}$ is expected, which should be compensated for by a year of extra running at the same luminosity, with respect to the case of higher mass resolution.

So far we have assumed a 100% acceptance and detection efficiencies for j/l's in the final states, the same for b tagging. This is obviously completely unrealistic, and before drawing definite conclusions a full analysis (including kinematical cuts, detector efficiencies, hadronization effects, etc.) should be done. We adopt here the set of kinematical cuts given in Ref. [38]. As the substantial part of Higgs signals would come from reaction (1), which furthermore is the most affected by competitive backgrounds [contrary to processes (2)–(3), which are virtually free from backgrounds in the region where Higgs signals can be disentangled, $M_\phi \neq M_{Z^0}$], we perform the study for the case $W^{\pm}\phi X$ and for the corresponding (continuum) backgrounds.

If we assume as acceptance region the one defined by[15] transverse momentum p_T^i of at least 20 GeV, pseudorapidity $|\eta_i|$ less than 4.5, and separation $\Delta R_{ij} = \sqrt{\Delta\eta_{ij}^2 + \Delta\varphi_{ij}^2} > 1$; for all the ith and jth b's and jets of the signature $b\bar{b}jjX$, then the reduction factors for the $W^{\pm}\phi X$ signal and the tbX and $t\bar{t}X$ background rates are $R \approx 16$–7 (for $M_\phi = 60$–140 GeV), ≈ 14 and ≈ 11, respectively.

That means that, on the other hand, the number of events is reduced to a few units per year (from ≈ 3 at $M_\phi = 140$ GeV to ≈ 8 at $M_\phi = 60$ GeV, for hadronic $W^{\pm}$ decays) whereas, on the other hand, the effect on the significances is a reduction factor approximately equal to .4(2), for $M_\phi = 60(140)$ GeV. Therefore, we would conclude that even though these selection criteria act in the direction of favoring the backgrounds, largely spoiling the effectiveness of the $M_{bW\to bjj}$ cut, nevertheless, the final values we obtain for S, B and $S/\sqrt{B}$ shouldn't prevent the experimental feasibility of this analysis, but only imposing the requirement of accumulating a higher luminosity (in at least two years time), in order to clearly disentangle Higgs boson signals. In general, we would like to stress here that our choice of kinematical cuts could well be different from the one which will be at the end imposed by the real LEP⊗LHC detectors. At present, in fact, the acceptances of these latter have yet not been looked into, as even the most recent and complete studies on the argument only deal with simulations done for the LHC (see the ATLAS [55] and CMS [56] Technical Proposals). That is, we wonder if detectors designed for a pp machine will be the same and/or will work in the same configuration even when they will be set up around a different kind of machine, an ep collider. Nothing prevents us then from thinking that by the time the LEP⊗LHC collider will be operating both the improvement in the detection techniques and the necessity to design the detectors in view of their best performances at an ep machine could end up reducing the impact of the acceptance cuts on the event selection procedure.

Concerning flavor identification, it is clear that high b-tagging performances and excellent not-b rejection are needed, at least as the ones expected at the LHC in the pp mode [18].

Before concluding, we notice here how processes like (1)–(3) could turn out to be extremely interesting if one considers their counterparts, e.g., in the minimal supersymmetric standard model (MSSM). Here quark-Higgs couplings proportional to $\tan\beta$ can enhance the signals up to ~ 1000 times for very large $\tan\beta$. This drastic enhancement happens when considering the contribution of diagrams involving the bremsstrahlung of the pseudoscalar boson A^0 off massive *down*-type quarks (i.e., b quarks: hence masses should be included). This occurs in all the Feynman diagrams of process (3), while it only happens for the suppressed graphs 1–6 [and 9,10] in (2)[(1)]. These latter contribute to the total rate at the level of % for the SM case but are the only surviving ones for the MSSM (since the pseudoscalar boson A^0 does not couple to vector bosons at tree level). In addition, in processes (1)–(3), once we substitute ϕ by one of the MSSM neutral Higgses H^0, h^0, and A^0 and we also include the flavor changing cases in which $\phi \leftrightarrow H^{\pm}$ and double Higgs productions in $q\gamma$ fusion ($W^{\pm} \leftrightarrow H^{\pm}$ and $Z^0 \leftrightarrow H^0, h^0, A^0$), we will have a very rich laboratory where all the fundamental interactions of the MSSM can be carefully studied. A complete analysis within this model is presented in the following paper [57].

[15] In the case of the signal no requirement is imposed on the spectator jet from the q' quark in (1).

SUMMARY AND CONCLUSIONS

In summary, we have studied the production cross sections of the SM Higgs ϕ with mass in the range 60 GeV $\lesssim M_\phi \lesssim$ 140 GeV at a next-generation ep collider, with 500 GeV $\lesssim \sqrt{s_{ep}} \lesssim 3$ TeV, through the partonic processes

$$\gamma q(\bar{q}) \to q'(\bar{q}')W^{\pm}\phi \,,$$

$$\gamma q(\bar{q}) \to q(\bar{q})Z^0\phi \,,$$

and

$$g\gamma \to q\bar{q}\phi \,,$$

for all possible (massive) flavors of the quarks $q(q')$, with incoming photons generated via Compton back scattering of laser light.

Special attention has been devoted to the case of the planned CERN LEP⊗LHC ep collider (with $\sqrt{s_{ep}} \approx 1.36$ TeV), where signatures in which the Higgs decays to $b\bar{b}$ pairs were studied, exploiting the possibilities given by b-tagging techniques.

We concluded that at this machine, apart from the case $M_\phi \approx M_{Z^0}$ which is impossible to disentangle, Higgs signals should be detectable above all the possible backgrounds over the most part of the remaining intermediate mass range, by searching for the hadronic decays of $W^{\pm}$'s in process (1), in particular after approximately a couple of years running at the luminosity $\mathcal{L} = 3$ fb^{-1} if $M_\phi \lesssim 120$ GeV. Because of the fact that the leptonic decay channels of the $W^{\pm}$'s give small rates and that a cut in the invariant mass M_{bW} is not applicable in this case, no possibility of detections exists if $W^{\pm} \to l\bar{\nu}_l$. Therefore, in this respect, we disagree with the conclusions given in Ref. [41]. In the case of processes (2)–(3), after the acceptance cuts here adopted we expect to get significant number of events only for a value of $\mathcal{L}$ much bigger than the one assumed here (more than an order of magnitude).

In general, if the LHC detectors will not be able to achieve the necessary performances for all the foreseen Higgs measurements, then the LEP⊗LHC collider option could provide interesting prospects of studying the SM Higgs boson parameters (i.e., M_ϕ, Γ_ϕ, BR's, etc.) in the intermediate mass range, in an environment partially

free from the QCD background typical of $pp/p\bar{p}$ accelerators, especially if larger b-tagging performance and/or a high luminosity can be achieved, in advance of a possible future NLC.

ACKNOWLEDGMENTS

We are grateful to J. B. Tausk for interesting discussions and useful suggestions, to T. Stelzer for his helpful advice on using MadGraph, and to W. J. Stirling for reading the manuscript.

APPENDIX

In this section we present the explicit formulas for the helicity amplitudes of the signal processes we have studied. Definitions of S, Y, and Z functions and of other quantities (p, λ, μ, η, etc.), which enter in the following, can be found in Ref. [58], with identical notation.

Here, we introduce the definitions

$$-b_1 = -b_2 = b_3 = 2b_4 = 2b_5 = 2b_6 = 2b_7 = 1 \quad \text{(A1)}$$

for the coefficients of the incoming or outgoing four-momenta,

$$D_V(p) = \frac{1}{p^2 - M_V^2} \ , \quad D_q(p) = \frac{1}{p^2 - m_q^2} \quad \text{(A2)}$$

for the propagators, where $V = W^{\pm}, Z^0$ and $q = u$ or d,

$$N_i = [4(p_i \cdot q_i)]^{-1/2} \ , \quad i = 1,2 \quad \text{(A3)}$$

for the gluon ($i = 1$) and photon ($i = 2$) normalization factor, where $p_i(q_i)$ is the massless vector four-momentum (any four-vector not proportional to p_i), with $i = 1,2$ [43]. The symbols r_1 and r_2 represent two light-like four-momenta satisfying the relations

$$r_1^2 = r_2^2 = 0 \ , \quad r_1^\mu + r_2^\mu = p_4^\mu \ , \quad \text{(A4)}$$

($d\Omega_{r_1(r_2)}$ indicates the solid angle of $r_{1(2)}$ in the rest frame of p_4) [43], p_6 and p_7 are antispinor four-momenta such that

$$p_6^\mu \equiv p_4^\mu \ , \quad p_7^\mu \equiv p_5^\mu \ , \quad \text{(A5)}$$

and

$$\sum_{\lambda=\pm} u(p_i,\lambda)\bar{u}(p_i,\lambda) = \not{p}_i - m_i \ , \quad \text{with } i = 6,7 \ , \quad \text{(A6)}$$

while

$$\sum_{\lambda=\pm} u(p_i,\lambda)\bar{u}(p_i,\lambda) = \not{p}_i + m_i \ , \quad \text{with } i = 4,5 \ . \quad \text{(A7)}$$

We also define the spinor functions[16]

$$\begin{aligned}
\mathcal{X}_2 &= \sum_{\lambda=\pm} \sum_{i=1,3} (-b_i) Y([2];[i];1,1) Y([i];(2);1,1) \ , \\
\mathcal{X}_4 &= \sum_{\lambda=\pm} \sum_{i=5,7} b_i Y(\{1\};[i];1,1) Y([i];\{2\};1,1) \ , \\
\mathcal{X}_{31}^{qV(\prime)} &= \sum_{\lambda=\pm} \sum_{i=4,6(5,7)} b_i Y([3];[i];1,1) Y([i];[1];c_{R_V}^q, c_{L_V}^q) \ , \\
\mathcal{Y}_2^{(\prime)} &= \sum_{\lambda=\pm} \sum_{i=4,6(5,7)} b_i Y([2];[i];1,1) Y([i];(2);1,1) \ , \\
\mathcal{Y}_4 &= \sum_{\lambda=\pm} Y(\{1\};p_2,\lambda;1,1) Y(p_2,\lambda;\{2\};1,1) \ , \\
\mathcal{F}_{31}^{qV} &= \mu_1\eta_1 Y([3];[1];c_{L_V}^q, c_{R_V}^q) - \mu_3\eta_3 Y([3];[1];c_{R_V}^q, c_{L_V}^q) \ , \\
\mathcal{Y}_{31}^{qV} &= \sum_{\lambda=\pm} Y([3];p_2,\lambda;1,1) Y(p_2,\lambda;[1];c_{R_V}^q, c_{L_V}^q) \ , \\
\tilde{\mathcal{Y}}_{31}^{qV} &= \mathcal{Y}_{31}^{qV} - \frac{\mathcal{F}_{31}^{qV}}{M_V^2} p_2 \cdot (p_4 + p_5) \ , \\
\mathcal{Z}_{24} &= Z([2];(2);\{1\};\{2\};1,1;1,1) \ , \\
\mathcal{Z}_{312}^{qV} &= Z([3];[1];[2];(2);c_{R_V}^q, c_{L_V}^q;1,1) \ , \\
\tilde{\mathcal{Z}}_{312}^{qV} &= \mathcal{Z}_{312}^{qV} - \frac{\mathcal{F}_{31}^{qV}}{M_V^2} (\mathcal{Y}_2 + \mathcal{Y}_2') \ , \\
\mathcal{Z}_{314}^{qV} &= Z([3];[1];\{1\};\{2\};c_{R_V}^q, c_{L_V}^q;1,1) \ , \\
\tilde{\mathcal{Z}}_{314}^{qV} &= \mathcal{Z}_{314}^{qV} - \frac{\mathcal{F}_{31}^{qV}}{M_V^2} (\mathcal{X}_4 - \mathcal{Y}_4) \ ,
\end{aligned} \quad \text{(A8)}$$

[16]Throughout this Appendix we adopt the symbol $\{\lambda\}$ to denote a set of helicities of all external particles in a given reaction, $\sum_{\{\lambda\}}$ to indicate the usual sum over all their possible combinations, and the symbol $\sum_{i=j,k,l,\ldots}$ to indicate a sum over $j,k,l,\ldots$ with index i.

TABLE VI. SM Higgs boson $\mathcal{H}$ couplings to the gauge bosons $W^\pm$ and Z^0.

	ϕ
$W^\pm W^\mp$	$\frac{M_{W^\pm}}{s_W}$
$Z^0 Z^0$	$\frac{M_{W^\pm}}{s_W c_W^2}$

where V represents a gauge boson $W^\pm, Z^0$ or $\gamma, q = u$ or d (u- and d-type quarks of arbitrary masses m_u and m_d, respectively), and with the shorthand notations $[x] = p_x, \lambda_x$ $(x = 1, \dots 4)$, $(x) = q_x, \lambda_x$ $(x = 1, 2)$, and $\{x\} = r_x, -(x = 1, 2)$.

In the following we adopt $[i] = p_i, \lambda$ and $[j] = p_j, \lambda'$, whereas the couplings c_R, c_L, and $\mathcal{H}$ can be easily deduced from Tables VI and VII. Also, we sometimes make use of the equalities

$$\mathcal{Y}_2 + \mathcal{Y}_2' = \mathcal{X}_2 \ , \quad \mathcal{X}_{31}^{qV} + \mathcal{X}_{31}^{qV\prime} = \mathcal{Y}_{31}^{qV} + \mathcal{F}_{31}^{qV} \ . \tag{A9}$$

1. Process $d\gamma \to uW^-\phi$

In order to obtain from Fig. 1 the Feynman graphs of the process

TABLE VII. SM right and left handed couplings (c_R, c_L) of u- and d-type quarks to the neutral gauge bosons g, γ, Z^0, to the charged $W^\pm$'s and to the Higgs boson ϕ. We have $g_R^q = -Q^q s_W^2$ and $g_L^q = T_3^q - Q^q s_W^2 (q = u, d)$, with $(Q^u, T^u) = (+\frac{2}{3}, \frac{1}{2})$ and $(Q^d, T_3^d) = (-\frac{1}{3}, -\frac{1}{2})$ for quark charges and isospins.

g	γ	Z^0	$W^\pm$	ϕ
(1,1)	$Q^q(1,1)$	$\frac{1}{s_W c_W}(g_R^q, g_L^q)$	$\frac{1}{\sqrt{2}s_W}(0,1)$	$\frac{m_q}{2M_{W^\pm} s_W}(1,1)$

$$d(p_1, \lambda_1) + \gamma(p_2, \lambda_2) \to u(p_3, \lambda_3) + W^-(p_4) + \phi(p_5) \ , \tag{A10}$$

one has to make the following assignments:

$$q = d \ , \quad q' = u \ , \quad V^{(*)} = W^{\pm(*)} \ . \tag{A11}$$

The corresponding matrix element, summed over final spins and averaged over initial ones, is given by

$$|\bar{M}| = \frac{e^6}{4} N_2^2 \frac{3}{8\pi M_{W^\pm}^2} \sum_{\{\lambda\}} \int d\Omega_{r_1(r_2)} \sum_{l,m=1}^{12} T_l^{\{\lambda\}} T_m^{\{\lambda\}*} \ , \tag{A12}$$

where

$$\begin{aligned}
iT_1^{\{\lambda\}} &= D_u(p_3+p_5)D_d(p_1+p_2)M_1^{\{\lambda\}}\mathcal{H}_1 \ , \quad iT_2^{\{\lambda\}} = D_d(p_3+p_4)D_d(p_1+p_2)M_2^{\{\lambda\}}\mathcal{H}_2 \ , \\
iT_3^{\{\lambda\}} &= D_d(p_3+p_4)D_d(p_1-p_5)M_3^{\{\lambda\}}\mathcal{H}_3 \ , \quad iT_4^{\{\lambda\}} = D_u(p_3+p_5)D_u(p_1-p_4)M_4^{\{\lambda\}}\mathcal{H}_4 \ , \\
iT_5^{\{\lambda\}} &= D_u(p_3-p_2)D_u(p_1-p_4)M_5^{\{\lambda\}}\mathcal{H}_5 \ , \quad iT_6^{\{\lambda\}} = D_u(p_3-p_2)D_d(p_1-p_5)M_6^{\{\lambda\}}\mathcal{H}_6 \ , \\
iT_7^{\{\lambda\}} &= D_{W^\pm}(p_4+p_5)D_d(p_1+p_2)M_7^{\{\lambda\}}\mathcal{H}_7 \ , \quad iT_8^{\{\lambda\}} = D_{W^\pm}(p_4+p_5)D_u(p_3-p_2)M_8^{\{\lambda\}}\mathcal{H}_8 \ , \\
iT_9^{\{\lambda\}} &= D_{W^\pm}(p_2-p_4)D_u(p_3+p_5)M_9^{\{\lambda\}}\mathcal{H}_9 \ , \quad iT_{10}^{\{\lambda\}} = D_{W^\pm}(p_2-p_4)D_d(p_1-p_5)M_{10}^{\{\lambda\}}\mathcal{H}_{10} \ , \\
iT_{11}^{\{\lambda\}} &= D_{W^\pm}(p_1-p_3)D_{W^\pm}(p_4+p_5)M_{11}^{\{\lambda\}}\mathcal{H}_{11} \ , \quad iT_{12}^{\{\lambda\}} = D_{W^\pm}(p_1-p_3)D_{W^\pm}(p_2-p_4)M_{12}^{\{\lambda\}}\mathcal{H}_{12} \ .
\end{aligned} \tag{A13}$$

We have

$$\begin{aligned}
M_1^{\{\lambda\}} &= \sum_{\lambda=\pm}\sum_{\lambda'=\pm}\sum_{i=3,5,7}\sum_{j=1,2}(-b_i b_j)Y([3];[i];c_{R_\phi}^u, c_{L_\phi}^u) \\
&\quad \times Z([i];[j];\{1\};\{2\};c_{R_{W^\pm}}, c_{L_{W^\pm}};1,1)Z([j];[1];[2];(2);c_{R_\gamma}^d, c_{L_\gamma}^d;1,1) \ , \\
M_2^{\{\lambda\}} &= \sum_{\lambda=\pm}\sum_{\lambda'=\pm}\sum_{i=3,4,6}\sum_{j=1,2}(-b_i b_j)Z([3];[i];\{1\};\{2\};c_{R_{W^\pm}}, c_{L_{W^\pm}};1,1) \\
&\quad \times Y([i];[j];c_{R_\phi}^d, c_{L_\phi}^d)Z([j];[1];[2];(2);c_{R_\gamma}^d, c_{L_\gamma}^d;1,1) \ , \\
M_3^{\{\lambda\}} &= \sum_{\lambda=\pm}\sum_{\lambda'=\pm}\sum_{i=3,4,6}\sum_{j=1,5}(-b_i b_j)Z([3];[i];\{1\};\{2\};c_{R_{W^\pm}}, c_{L_{W^\pm}};1,1) \\
&\quad \times Z([i];[j];[2];(2);c_{R_\gamma}^d, c_{L_\gamma}^d;1,1)Y([j];[1];c_{R_\phi}^d, c_{L_\phi}^d) \ , \\
M_4^{\{\lambda\}} &= \sum_{\lambda=\pm}\sum_{\lambda'=\pm}\sum_{i=3,5,7}\sum_{j=1,4,6}(-b_i b_j)Y([3];[i];c_{R_\phi}^u, c_{L_\phi}^u) \\
&\quad \times Z([i];[j];[2];(2);c_{R_\gamma}^u, c_{L_\gamma}^u;1,1)Z([j];[1];\{1\};\{2\};c_{R_{W^\pm}}, c_{L_{W^\pm}};1,1) \ , \\
M_5^{\{\lambda\}} &= \sum_{\lambda=\pm}\sum_{\lambda'=\pm}\sum_{i=3,2}\sum_{j=1,4,6}(-b_i b_j)Z([3];[i];[2];(2);c_{R_\gamma}^u, c_{L_\gamma}^u;1,1) \\
&\quad \times Y([i];[j];c_{R_\phi}^u, c_{L_\phi}^u)Z([j];[1];\{1\};\{2\};c_{R_{W^\pm}}, c_{L_{W^\pm}};1,1) \ , \\
M_6^{\{\lambda\}} &= \sum_{\lambda=\pm}\sum_{\lambda'=\pm}\sum_{i=3,2}\sum_{j=1,5,7}(-b_i b_j)Z([3];[i];[2];(2);c_{R_\gamma}^u, c_{L_\gamma}^u;1,1) \\
&\quad \times Z([i];[j];\{1\};\{2\};c_{R_{W^\pm}}, c_{L_{W^\pm}};1,1)Y([j];[1];c_{R_\phi}^d, c_{L_\phi}^d) \ ,
\end{aligned}$$

$$M_7^{\{\lambda\}} = \sum_{\lambda=\pm}\sum_{i=1,2}(-b_i)Z([i];[1];[2];(2);c^d_{R_\gamma},c^d_{L_\gamma};1,1)$$
$$\times\Bigg\{Z([3];[i];\{1\};\{2\};c_{R_{W^\pm}},c_{L_{W^\pm}};1,1)$$
$$-\frac{\mathcal{X}_4}{M^2_{W^\pm}}\left[\sum_{\lambda'=\pm}\sum_{j=1,2,3}(-b_j)Y([3];[j];1,1)Y([j];[i];c_{R_{W^\pm}},c_{L_{W^\pm}})\right]\Bigg\},$$
$$M_8^{\{\lambda\}} = \sum_{\lambda=\pm}\sum_{i=2,3}(b_i)Z([3];[i];[2];(2);c^u_{R_\gamma},c^u_{L_\gamma};1,1)$$
$$\times\Bigg\{Z([i];[1];\{1\};\{2\};c_{R_{W^\pm}},c_{L_{W^\pm}};1,1)$$
$$-\frac{\mathcal{X}_4}{M^2_{W^\pm}}\left[\sum_{\lambda'=\pm}\sum_{j=1,2,3}(-b_j)Y([i];[j];1,1)Y([j];[1];c_{R_{W^\pm}},c_{L_{W^\pm}})\right]\Bigg\},$$
$$M_9^{\{\lambda\}} = \sum_{\lambda=\pm}\sum_{i=3,5,7}(2b_i)Y([3];[i];c^u_{R_\phi},c^u_{L_\phi})$$
$$\times\Bigg[\mathcal{Z}_{24}\sum_{\lambda'=\pm}Y([i];p_2,\lambda';1,1)Y(p_2,\lambda';[1];c_{R_{W^\pm}},c_{L_{W^\pm}})$$
$$-\mathcal{Y}_2Z(\{1\};\{2\};[i];[1];1,1;c_{R_{W^\pm}},c_{L_{W^\pm}})-\mathcal{Y}_4Z([2];(2);[i];[1];1,1;c_{R_{W^\pm}},c_{L_{W^\pm}})\Bigg],$$
$$M_{10}^{\{\lambda\}} = \sum_{\lambda=\pm}\sum_{i=1,5,7}(-2b_i)Y([i];[1];c^d_{R_\phi},c^d_{L_\phi})$$
$$\times\Bigg[\mathcal{Z}_{24}\sum_{\lambda'=\pm}Y([3];p_2,\lambda';1,1)Y(p_2,\lambda';[i];c_{R_{W^\pm}},c_{L_{W^\pm}})$$
$$-\mathcal{Y}_2Z(\{1\};\{2\};[3];[i];1,1;c_{R_{W^\pm}},c_{L_{W^\pm}})-\mathcal{Y}_4Z([2];(2);[3];[i];1,1;c_{R_{W^\pm}},c_{L_{W^\pm}})\Bigg],$$
$$M_{11}^{\{\lambda\}} = \mathcal{Z}_{24}(\mathcal{F}^{W^\pm}_{31}+2\mathcal{Y}^{W^\pm}_{31})-2\mathcal{X}_2\tilde{\mathcal{Z}}^{W^\pm}_{314}-(2\mathcal{Y}_4-\mathcal{X}_4)\tilde{\mathcal{Z}}^{W^\pm}_{312}$$
$$-\frac{1}{M^2_{W^\pm}}[\mathcal{X}_2\mathcal{X}_4(\mathcal{Y}^{W^\pm}_{31}-\mathcal{X}^{W^\pm}_{31}-\mathcal{X}^{W^{\pm\prime}}_{31})+(p_1-p_3)^2(\mathcal{Z}_{24}\mathcal{F}^{W^\pm}_{31}+\tilde{\mathcal{Z}}^{W^\pm}_{312}\mathcal{X}_4)+2p_2\cdot(p_1-p_3)\mathcal{Z}_{24}\mathcal{F}^{W^\pm}_{31}]$$
$$-\frac{1}{M^4_{W^\pm}}\{[(p_1-p_3)^2+p_2\cdot(p_1-p_3)]\mathcal{X}_4(\mathcal{Y}_2-\mathcal{Y}_2')\mathcal{F}^{W^\pm}_{31}\},$$
$$M_{12}^{\{\lambda\}} = 2(\tilde{\mathcal{Y}}^{W^\pm}_{31}\mathcal{Z}_{24}-\mathcal{Y}_2\tilde{\mathcal{Z}}^{W^\pm}_{314}-\mathcal{Y}_4\tilde{\mathcal{Z}}^{W^\pm}_{312}). \tag{A14}$$

2. Process $d\gamma \to dZ^0\phi$

The Feynman graphs for the process

$$d(p_1,\lambda_1)+\gamma(p_2,\lambda_2)\to d(p_3,\lambda_3)+Z^0(p_4)+\phi(p_5), \tag{A15}$$

can be obtained from Fig. 1 by setting

$$q=q'=d,\quad V^{(*)}=Z^{0(*)}. \tag{A16}$$

The formulas for the amplitude squared are practically the same as in the previous section, considering the first 8 amplitudes only (i.e., $M_i^{\{\lambda\}}=0$ for $i=9,\ldots,12$), with the relabeling:

$$u\to d,\quad W^\pm\to Z^0, \tag{A17}$$

in Eqs. (A12)–(A14).

3. Process $g\gamma \to u\bar{u}\phi$

The Feynman diagrams for

$$g(p_1,\lambda_1)+\gamma(p_2,\lambda_2)\to u(p_3,\lambda_3)+\bar{u}(p_4,\lambda_4)+\phi(p_5), \tag{A18}$$

are shown in Fig. 2, where $q=u$. The amplitude squared is

$$|\bar{M}|=\frac{e^4g_s^2}{4}N_1^2N_2^2\sum_{\{\lambda\}}\sum_{l,m=1}^{6}T_l^{\{\lambda\}}T_m^{\{\lambda\}*}. \tag{A19}$$

The expressions for the $T_i^{\{\lambda\}}$'s are

$$-iT_1^{\{\lambda\}} = D_u(p_3+p_5)D_u(p_1-p_4)M_1^{\{\lambda\}}\mathcal{H}_1 \ , \quad -iT_2^{\{\lambda\}} = D_u(p_3-p_2)D_u(p_1-p_4)M_2^{\{\lambda\}}\mathcal{H}_2 \ ,$$
$$-iT_3^{\{\lambda\}} = D_u(p_3-p_2)D_u(p_4+p_5)M_3^{\{\lambda\}}\mathcal{H}_3 \ ,$$
$$-iT_{i+3}^{\{\lambda\}} = -iT_i^{\{\lambda\}}(p_3 \leftrightarrow p_4) \ , \quad i=1,\ldots,3 \ , \tag{A20}$$

while the spinor functions are

$$\begin{aligned}
M_1^{\{\lambda\}} &= \sum_{\lambda=\pm}\sum_{\lambda'=\pm}\sum_{i=3,5,7}\sum_{j=1,4}(-b_ib_j)Y([3];[i];c^u_{R_\phi},c^u_{L_\phi}) \\
&\quad \times Z([i];[j];[2];(2);c^u_{R_\gamma},c^u_{L_\gamma};1,1)Z([j];[4];[1];(1);c^u_{R_g},c^u_{L_g};1,1) \ , \\
M_2^{\{\lambda\}} &= \sum_{\lambda=\pm}\sum_{\lambda'=\pm}\sum_{i=2,3}\sum_{j=1,4}(-b_ib_j)Z([3];[i];[2];(2);c^u_{R_\gamma},c^u_{L_\gamma};1,1) \\
&\quad \times Y([i];[j];c^u_{R_\phi},c^u_{L_\phi})Z([j];[4];[1];(1);c^u_{R_g},c^u_{L_g};1,1) \ , \\
M_3^{\{\lambda\}} &= \sum_{\lambda=\pm}\sum_{\lambda'=\pm}\sum_{i=2,3}\sum_{j=4,5,7}(-b_ib_j)Z([3];[i];[2];(2);c^u_{R_\gamma},c^u_{L_\gamma};1,1) \\
&\quad \times Z([i];[j];[1];(1);c^u_{R_g},c^u_{L_g};1,1)Y([j];[4];c^u_{R_\phi},c^u_{L_\phi}) \ , \\
M_{i+3}^{\{\lambda\}} &= M_i^{\{\lambda\}}(p_3 \leftrightarrow p_4) \ , \quad i=1,\ldots,3 \ .
\end{aligned} \tag{A21}$$

By trivial relabeling and sign exchanges, it is possible to obtain from the above formulas the corresponding ones for the u-type quark initiated processes

$$\begin{aligned}
u\gamma &\to dW^+\phi \ , \\
u\gamma &\to uZ^0\phi \ ,
\end{aligned} \tag{A22}$$

as for the charge conjugate reactions

$$\begin{aligned}
\bar{d}\gamma &\to \bar{u}W^+\phi \ , \\
\bar{d}\gamma &\to \bar{d}Z^0\phi \ .
\end{aligned} \tag{A23}$$

Finally, the same can be done for obtaining the helicity amplitudes for the g-initiated process

$$g\gamma \to d\bar{d}\phi \ . \tag{A24}$$

[1] S. L. Glashow, Nucl. Phys. **22**, 579 (1961); S. Weinberg, Phys. Rev. Lett. **19**, 1264 (1967); A. Salam, in *Elementary Particle Theory: Relativistic Groups and Analyticity (Nobel Symposium No. 8)*, edited by N. Svartholm (Almqvist and Wiksells, Stockholm, 1968), p. 367.

[2] P. W. Higgs, Phys. Rev. Lett. **12**, 132 (1964).

[3] ALEPH Collaboration, D. Decomp *et al.*, Phys. Rep. **216**, 253 (1992); DELPHI Collaboration, P. Aarnio *et al.*, Nucl. Phys. **B373**, 3 (1992); L3 Collaboration, B. Adeva *et al.*, Phys. Lett. B **303**, 391 (1993); OPAL Collaboration, M. Akrawy *et al.*, *ibid.* **253**, 511 (1991).

[4] M. Veltman, Phys. Lett. **70B**, 253 (1977).

[5] B. W. Lee, C. Quigg, and G. B. Thacker, Phys. Rev. Lett. **38**, 883 (1977); Phys. Rev. D **16**, 1519 (1977).

[6] *Proceedings of the ECFA Workshop on LEP 200*, Aachen, West Germany, 1986, edited by A. Bohm and W. Hoogland (CERN Report No. 87-08, Geneva, Switzerland, 1987).

[7] *Proceedings of the ECFA Large Hadron Collider Workshop,* Aachen, Germany, edited by G. Jarlskog and D. Rein (CERN Report No. 90-10, ECFA Report No. 90-133, Geneva, Switzerland, 1990).

[8] J. D. Bjorken, *Proceedings of the Summer Institute on Particle Physics* (SLAC Report No. 198, 1976); B. W. Lee, C. Quigg, and H. B. Thacker, Phys. Rev. D **16**, 1519 (1977); J. Ellis, M. K. Gaillard, and D. V. Nanopoulos, Nucl. Phys. **B106**, 292 (1976); B. L. Ioffe and V. A. Khoze, Sov. J. Part. Nucl. **9**, 50 (1978).

[9] H. Georgi, S. L. Glashow, M. E. Machacek, and D. V. Nanopoulos, Phys. Rev. Lett. **40**, 692 (1978).

[10] R. N. Cahn and S. Dawson, Phys. Lett. **136B**, 196 (1984).

[11] S. L. Glashow, D. V. Nanopoulos, and A. Yildiz, Phys. Rev. D **18**, 1724 (1978).

[12] R. Kleiss, Z. Kunszt, and W. J. Stirling, Phys. Lett. B **253**, 269 (1991); SDC Collaboration, M. L. Mangano, Report No. *SSC-SDC-90-00113* (unpublished).

[13] R. Raitio and W. W. Wada, Phys. Rev. D **19**, 941 (1979); J. N. Ng and P. Zakarauskas, *ibid.* **29**, 876 (1984).

[14] J. F. Gunion, Phys. Lett. B **261**, 510 (1991); W. J. Marciano and F. E. Paige, Phys. Rev. Lett. **66**, 2433 (1991); A. Ballestrero and E. Maina, Phys. Lett. B **268**, 437 (1992); Z. Kunzst, Z. Trócsányi, and W. J. Stirling, *ibid.* **271**, 247 (1991); D. J. Summers, *ibid.* **277**, 366 (1992).

[15] C. Seez *et al.*, in Ref. [7].
[16] J. Dai, J. F. Gunion, and R. Vega, Phys. Rev. Lett. **71**, 2699 (1993).
[17] E. L. Berger *et al.*, "Solenoidal Detector Collaboration Technical Design Report," Report No. SDC-92-201, SSCL-SR-1215, 1992 (unpublished).
[18] D. Froidevaux and E. Richter-Was, Z. Phys. C **67**, 213 (1995).
[19] J. F. Gunion, H. E. Haber, G. L. Kane, and S. Dawson, *The Higgs Hunter Guide* (Addison-Wesley, Reading, MA, 1990).
[20] *Physics and Experiments with Linear Colliders,* Proceedings of the Workshop, Saariselkä, Finland, 1991, edited by R. Orawa, P. Eerola, and M. Nordberg (World Scientific, Singapore, 1992).
[21] e^+e^- *Collisions at 500 GeV: The Physics Potential,* Proceedings of the Workshop, Munich, Annecy, Hamburg, 1991, edited by P. M. Zerwas (DESY Report No. 92-123A/B/C, Hamburg, 1992).
[22] e^+e^- *Linear Colliders LC92,* Proceedings of the ECFA workshop, Garmisch Partenkirchen, 1992, edited by R. Settles (Report Nos. MPI-PhE/93-14, ECFA 93-154).
[23] *Proceedings of the First Workshop on Japan Lindear Collider (JLC),* Tsukuba, Japan, 1989, edited by S. Kawabata (KEK Report No. 90-2, Tsukuba, 1990); *Proceedings of the Second Workshop on Japan Linear Collider (JLC),* Tsukuba, Japan, 1990, edited by S. Kawabata (KEK Report No. 91-10, Tsukuba, 1991).
[24] V. Barger, K. Cheung, A. Djouadi, B. A. Kniehl, and P. M. Zerwas, Phys. Rev. D **49**, 79 (1994).
[25] D. R. T. Jones and S. T. Petkov, Phys. Lett. **84B**, 440 (1979); R. N. Cahn and S. Dawson, *ibid.* **136B**, 196 (1984); K. Hikasa, *ibid.* **164B**, 341 (1985); G. Altarelli, B. Mele, and F. Pitolli, Nucl. Phys. **B287**, 205 (1987); B. Kniehl, Z. Phys. C. **55**, 605 (1992).
[26] V. Barger, K. Cheung, B. A. Kniehl, and R. J. Phillips, Phys. Rev. D **46**, 3725 (1992).
[27] K. Hagiwara, J. Kanzaki, and H. Murayama, Durham Univ. Report No. DTP-91-18, 1991 (unpublished).
[28] J. F. Gunion and H. E. Haber, *1990 DPF Summer Study on High Energy Physics,* Snowmass, Colorado, 1990 (Report No. UCD-90-25, 1990); J. F. Gunion and H. E. Haber, in *Research Directions for the Decade,* Proceedings of the Summer Study, Snowmass, Colorado, 1990, edited by E. L. Berger (World Scientific, Singapore, 1991); J. F. Gunion and H. E. Haber, Phys. Rev. D **48**, 5109 (1993).
[29] D. Borden, D. Bauer, and D. Caldwell, SLAC Report No. SLAC-PUB-5715, 1992 (unpublished); F. Richard, in Ref. [21]; D. Bowser-Chao and K. Cheung, Phys. Rev. D **48**, 89 (1993).
[30] K. Cheung, Phys. Rev. D **47**, 3750 (1993); E. Boos, I. Ginzburg, K. Melnikov, T. Sack, and S. Shichanin, Z. Phys. C **56**, 487 (1992).
[31] E. Boos, M. Dubinin, V. Ilyin, A. Pukhov, G. Jikia, and S. Sultanov, Phys. Lett. B **273**, 173 (1991).
[32] K. Hagiwara, I. Watanabe, and P. M. Zerwas, Phys. Lett. B **278**, 187 (1992).
[33] K. Cheung, Phys. Rev. D **48**, 1035 (1993).
[34] O. J. P. Eboli and M. C. Gonzales-Garcia, Phys. Rev. D **49**, 91 (1994).
[35] Proceedings of the HERA Workshop, edited by R. D. Peccei, Desy, Hamburg, 1987 (unpublished); Proceedings of the HERA Workshop, edited by W. Buchmüller and G. Ingelman, Desy, Hamburg, 1991 (unpublished).
[36] K. J. F. Gaemers, R. M. Godbole, and M. van der Horst, in Ref. [35] (1987).
[37] K. Hikasa, Particle Data Book, Phys. Rev. D **45**, 11-II (1992).
[38] G. Grindhammer, D. Haidt, J. Ohnemus, J. Vermaseren, and D. Zeppenfeld, in Ref. [7].
[39] T. Han and C. Liu, Z. Phys. C **28**, 295 (1985); D. A. Dicus and S. Willenbrock, Phys. Rev. D **32**, 1642 (1985).
[40] J. Blumlein, G. J. van Oldenborgh, and R. Ruckl, Nucl. Phys. **B395**, 35 (1993).
[41] K. Cheung, Phys. Lett. B **319**, 244 (1993).
[42] B. Grzadkowski, S. Pokorski, and J. Rosiek, Phys. Lett. B **272**, 143 (1991).
[43] R. Kleiss and W. J. Stirling, Nucl. Phys. **B262**, 235 (1985).
[44] C. Mana and M. Martinez, Nucl. Phys. **B287**, 601 (1987).
[45] K. Hagiwara and D. Zeppenfeld, Nucl. Phys. **B274**, 1 (1986).
[46] P. N. Harriman, A. D. Martin, R. G. Roberts, and W. J. Stirling, Phys. Rev. D **42**, 798 (1990).
[47] A. D. Martin, R. G. Roberts, and W. J. Stirling, Phys. Rev. D **50**, 6734 (1994).
[48] G. P. Lepage, J. Comput. Phys. **27**, 192 (1978).
[49] V. Telnov, Nucl. Instrum. Methods A **294**, 72 (1990); I. Ginzburg, G. Kotkin, V. Serbo, and V. Telnov, Nucl. Instrum. Methods A **205**, 47 (1983); **219**, 5 (1984).
[50] CDF Collaboration, F. Abe *et al.*, Phys. Rev. D **50**, 2966 (1994); Phys. Rev. Lett. **73**, 225 (1994).
[51] Z. Kunszt and W. J. Stirling, in Ref. [7]; P. M. Zerwas, in Ref. [22].
[52] T. Stelzer and W. F. Long, Comput. Phys. Commun. **81**, 357 (1994).
[53] E. Murayama, I. Watanabe, and K. Hagiwara, "HELAS:HELicity Amplitude Subroutines for Feynman Diagram Evaluations," KEK Report No. 91-11, 1992 (unpublished).
[54] U. Baur and J. J. Van der Bij, Nucl. Phys. **B304**, 451 (1988).
[55] ATLAS Technical Proposal, CERN/LHC/94-43 LHCC/P2, December 1994.
[56] CMS Technical Proposal, CERN/LHC/94-43 LHCC/P1, December 1994.
[57] G. Abu Leil and S. Moretti, following paper, Phys. Rev. D **53**, 178 (1996).
[58] S. Moretti, Phys. Rev. D **50**, 2016 (1994).